ROYAL SOCIETY OPEN SCIENCE

rsos.royalsocietypublishing.org

Research

**Cite this article:** Vasudevan S, Prabhune AA. 2018 Photophysical studies on curcumin-sophorolipid nanostructures: applications in quorum quenching and imaging. *R. Soc. open sci.* **5**: 170865. http://dx.doi.org/10.1098/rsos.170865

Received: 8 July 2017
Accepted: 4 January 2018

**Subject Category:**
Biochemistry and biophysics

**Subject Areas:**
biomaterials/biotechnology/microbiology

**Keywords:**
curcumin, sophorolipid, photophysical, quorum quenching

**Authors for correspondence:**
Asmita A. Prabhune
e-mail: aa.prabhune@ncl.res.in

Electronic supplementary material is available online at https://dx.doi.org/10.6084/m9.figshare.c.3982617.

THE ROYAL SOCIETY PUBLISHING

# Photophysical studies on curcumin-sophorolipid nanostructures: applications in quorum quenching and imaging

Sahana Vasudevan and Asmita A. Prabhune

Division of Biochemical Sciences, CSIR-National Chemical Laboratory, Dr. Homi-Bhabha Road, Pune 411008, India

SV, 0000-0002-8817-4704; AAP, 0000-0003-1839-2105

Sophorolipid biosurfactants are biodegradable, less toxic and FDA approved. The purified acidic form of sophorolipid is stimuli-responsive with self-assembling properties and used for solubilizing hydrophobic drugs. This study encapsulated curcumin (CU) with acidic sophorolipid (ASL) micelles and analysed using photophysical studies like UV-visible spectroscopy, photoluminescence (PL) spectroscopy and time-correlated single photon counting (TCSPC). TEM images have revealed ellipsoid micelles of approximately 100 nm size and were confirmed by dynamic light scattering. The bacterial fluorescence uptake studies showed the uptake of formed CUASL nanostructures into both Gram-positive and Gram-negative bacteria. They also showed quorum quenching activity against *Pseudomonas aeruginosa*. The results have demonstrated this system has potential theranostic applications.

## 1. Introduction

Biosurfactants, such as microbial glycolipids, are biodegradable, less toxic and can potentially be used to replace the conventional surfactant usage. They possess properties like anti-microbial [1], anti-biofilm [2] and anti-cancerous activity [3]. Additionally, self-assembling properties with the ability to mimic the cell membrane [4] allow them to be used as drug delivery vehicles.

Sophorolipids (SL) are a class of biosurfactants, produced by non-pathogenic yeast (predominantly *Starmerella bombicola*). Among the available biosurfactants, sophorolipids are an attractive choice because of their high yield (about 300–400 g $l^{-1}$) and can be produced from 'green' resources like oleic acid,

© 2018 The Authors. Published by the Royal Society under the terms of the Creative Commons Attribution License http://creativecommons.org/licenses/by/4.0/, which permits unrestricted use, provided the original author and source are credited.

rapeseed oil, linoleic acid, cetyl alcohol, etc. They have a wide range of applications such as household detergents, heavy metal removal, emulsifying agent in food process industry, cosmetic industry and are being extensively explored in the drug delivery applications [5]. The crude mixture of the sophorolipid has predominantly two forms—namely, lactonic and acidic. The ratio of these two forms is dependent on the culture conditions and fermentation time [6]. In applications such as nanoparticles synthesis [7], the accelerated gelation of the silk fibroin, the combinatorial roles of lactonic and acidic forms are well established [8,9].

Acidic sophorolipid (ASL), a bola amphiphile, confers a surfactant property to the crude sophorolipid. The two hydrophilic ends of a hydrophobic skeleton of oleic acid contain a sophorose and a carboxylic group. This makes ASL an excellent drug delivery vehicle similar to other bola amphiphiles [10]. ASL is a simple, water-soluble, mono-component, and stimuli-responsive molecule. Recently, interest in understanding the self-assembling properties of ASL has increased and has been studied in detail using techniques like nuclear magnetic resonance (NMR), small-angle neutron scattering (SANS) and molecular dynamics (MD) simulations. The pH and the concentration play a critical role in the morphology of the ASL micelles. At a $pH < 5$, the ASL micelles evolve from spherical to ellipsoidal as the concentration increases from 1 to 5 w/v% [11]. Empirical evidence has shown the ASL micellar structure to have three domains: (i) an aliphatic core, (ii) an outer hydrophilic shell that contains sophorose and COOH groups, (iii) palisade layer, which is a combination of sophorose, COOH, and an aliphatic region along with water [12]. The structural understanding has paved the way in modulating ASL for drug delivery applications specifically for encapsulating hydrophobic drug molecules such as curcumin [13,14].

Curcumin, a perennial rhizome, is an active compound obtained from *Curcuma longa* (turmeric). Curcumin is biological and pharmacological active. It acts as an anti-oxidant, anti-inflammatory [15], anti-microbial [16], neuroprotective [17], anti-malarial [18], anti-metastatic [19], anti-cancer [20], and anti-angiogenic component [21,22]. Despite these activities, the poor aqueous solubility, low bioavailability, enzymatic degradation and degradability at higher pH are the factors limiting its complete use as a polypharmacological agent. Hence, there is extensive research being carried out for making this non-toxic natural hydrophobic molecule, water soluble and bioavailable [23].

Solubilization of curcumin (CU), hydrophobic small drug molecule using acidic sophorolipid and the results on its improved anti-cancerous activity was already established [13]. The bioavailability of curcumin increased 150 times in Wistar rats in the presence of crude form of sophorolipid [14].

The above studies reveal that solubilization with sophorolipid led to the fluorescence of curcumin enhanced as a consequence of increased solubility. This finding motivated us to understand the mechanism of interaction between ASL and curcumin through photophysical analysis. The photophysical properties of curcumin are extensively studied in different solvents and systems like micelles [24–27], polymeric nanoparticles [28], cyclodextrin [29–31], bovine serum albumin [32,33], liposomes [34], microcapsules [35], nanocapsules [36] and polymeric systems [37]. It is well known that the photophysical properties of this chromophore are linked with the solvent environment and proton donating ability [38]. As curcumin is water-insoluble and aggregates, it shows an entirely different absorption and fluorescence peak as compared to the solubilized form [14]. The interaction of curcumin with various carrier systems can be very well understood with spectroscopic analysis. Hence photophysical studies were employed to analyse the stability and solubility of CUASL (Curcumin in ASL micellar environment).

The enhanced stable fluorescence of CUASL can be used as bioimaging tool for the diagnostic purpose. Curcumin and its analogues have been established as a fluorescent biomarker for confocal imaging [39] by uptake studies inside mammalian cells [40–44]. Curcumin is not yet reported as a biomarker for bacterial cells. Thus, the current study was carried out using sophorolipid (ASL) encapsulated curcumin as fluorescence tagging system in bacterial cells. This system showed easy uptake by *Escherichia coli* and *Staphylococcus aureus* and showed bright fluorescence in confocal microscopy.

It was observed from the confocal micrographs that the bacterial cells (both *E. coli* and *S. aureus*), were not damaged and that they remained intact after treatment with CUASL. The anti-bacterial action of curcumin damages and ruptures the cell membrane of the bacterial cells [45]. But in our case, the cells were not ruptured, which indicated that ASL facilitated the entry of curcumin for targeted action. Both curcumin and sophorolipid have anti-biofilm activity as well as anti-quorum sensing inhibition. Hence this study extended to evaluate the quorum quenching (QQ) ability of CUASL.

With an alarming increase in the anti-microbial resistance, targeting quorum sensing (QS) is considered to be a promising alternative therapy. QQ can be understood attenuating bacterial communication using natural and synthetic small molecules [46]. For our current studies, *Pseudomonas*

*aeruginosa*, a Gram-negative quorum sensing model organism, was tested. *Pseudomonas aeruginosa* operates through QS to infect immune-compromised patients leading to nosocomial infections. It communicates through two signal molecules, 3-oxo-C12-AHL and C4-AHL molecule [47]. Through quorum sensing, they have the ability to form biofilm and release exoproducts like pyocyanin and pyoverdine, rendering them resistant to most of the antibiotics [48]. Targeting QS signalling of *P. aeruginosa* is a promising alternative therapy to antibiotics. Curcumin as a QQ compound was first reported against *P. aeruginosa* PA01 in whole plant and animal models [49]. There are a few reports that established quorum quenching nature of curcumin against different Gram-negative quorum sensing pathogens [50–54]. Sophorolipids have also been shown to have anti-biofilm activity [2].

Here we report the entrapment of curcumin inside ASL micelles (CUASL) and analyse the stability using photophysical analysis in a concentration-dependent manner. The current studies reveal that at the optimum concentration of 5 w/v%, acidic sophorolipid can encapsulate curcumin. The solubility is achieved at the acidic pH, where curcumin is stable, thus reducing the degradation of curcumin. The decay kinetic profile follows triple exponential decay with an average decay time of 318.5 ps, revealing that curcumin may be present in the palisade layer of the acidic sophorolipid micelle. We have demonstrated quorum quenching activity against *P. aeruginosa* and fluorescent uptake studies for imaging bacterial cells like *E. coli* and *S. aureus*. Thus, leading a way for the development of soluble curcumin-based bioimaging system.

# 2. Material and methods

## 2.1. Purification of acidic sophorolipid

Resting cell method was adopted to synthesize oleic acid-derived sophorolipid (OASL) by *Starmerella bombicola* ATCC 22214 [5]. The extraction and purification protocol is explained in detail elsewhere [5]. ASL was purified using alkaline hydrolysis method [9], from the crude sophorolipid which is a combination of lactonic and acidic forms of sophorolipid [55]. The purity of the obtained ASL was confirmed using $H^1$ NMR-spectroscopy. The chemical structure of ASL is shown in figure 1*b*.

## 2.2. Synthesis of curcumin sophorolipid nanostructures

CU (figure 1*a*) was purchased from Sigma Aldrich (approx. 99% purity). Curcumin (1 mg ml$^{-1}$) was probe-sonicated for 40 min using Branson Digital Sonifier 250 together with different concentrations of ASL from 1 to 5 w/v% (above CMC = 0.11 mg ml$^{-1}$)[56].

## 2.3. Spectroscopic measurements

By keeping the concentration of curcumin constant (1 mg ml$^{-1}$), the absorption spectra at different ASL concentrations (1–5 w/v%) were recorded by the UV-1800 Shimadzu spectrophotometer with 10 mm quartz cell. The steady-state fluorescence was measured using Shimadzu RF-6000 Spectrofluorometer. CUASL was excited at the wavelength of 420 nm to record the emission spectrum.

To check the extent of degradation of curcumin inside the acidic sophorolipid micelles, the optical density (OD) of the maximum peak was recorded at the 0th and 60th min, at different concentrations of the micelle. The degradation percentage was calculated by the formula:

$$\%\ \text{degradation} = \left[\frac{\text{OD}_{0\ \text{min}} - \text{OD}_{60\ \text{min}}}{\text{OD}_{0\ \text{min}}}\right] \times 100. \tag{2.1}$$

## 2.4. Lifetime and quantum yield measurements

Time correlated single photon counting (TCSPC) spectrometer (Horiba Jobin Yvon IBH, UK) was used to collect time-resolved fluorescence measurements. The detailed description of the instrument is explained elsewhere [57]. In the present work, the excitation source used was a 400 nm diode laser (approx. 130 ps, 1 MHz repetition rate) and an MCP-PMT (microchannel plate–photomultiplier tube) detector was used for collecting the fluorescence signal. The analysis of the lifetime was done by using IBH DAS6 analysis software. For a good fit, the $\chi^2$ value was close to unity.

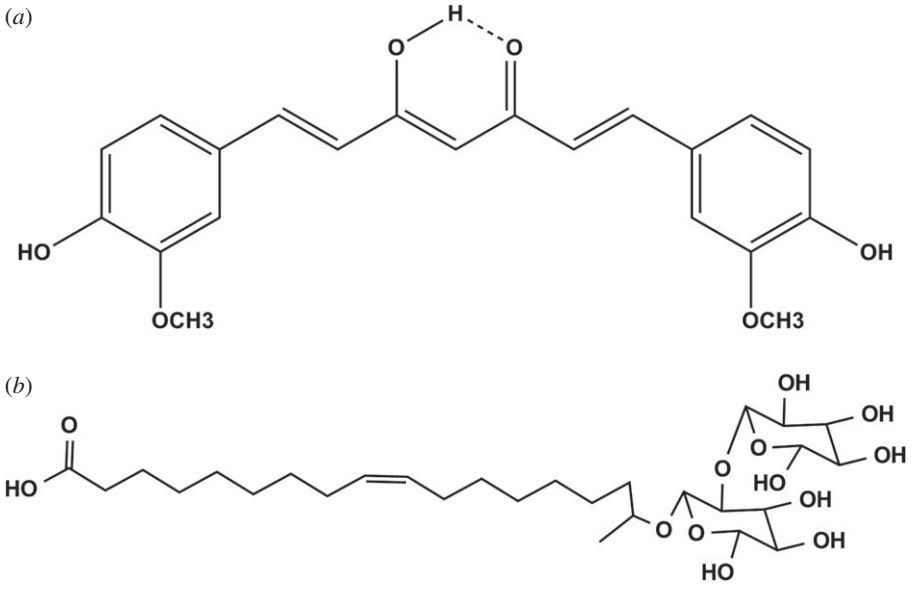


**Figure 1.** Chemical structures of (*a*) curcumin and (*b*) acidic sophorolipid.

The fluorescence quantum yield was calculated with quinine sulphate in 0.1 M $H_2SO_4$ (excitation wavelength= 350 nm) as a reference. Quantum yield was calculated by:

$$\Phi = (\Phi_R) \times \left(\frac{I}{I_R}\right) \times \left(\frac{A_R}{A}\right) \times \left(\frac{\eta^2}{\eta_R^2}\right), \tag{2.2}$$

where R refers to the reference. $\Phi$ and $\Phi_R$ are the quantum yields, $I$ and $I_R$ are the fluorescence intensities, $A$ and $A_R$ are the absorbances and $\eta$ and $\eta_R$ are the refractive index.

The average fluorescence lifetime is the sum of the product of the amplitudes and the respective lifetimes and was calculated using the equation (table 1):

$$\tau_{av} = a_1\tau_1 + a_2\tau_2 + a_3\tau_3. \tag{2.3}$$

The rate constants for the radiative decay ($k_r$) and non-radiative decay ($k_{nr}$) were calculated.

$$k_r = \frac{\Phi_f}{\tau_{av}} \tag{2.4}$$

and

$$k_{nr} = \left(\frac{1}{\tau_{av}}\right) - k_r. \tag{2.5}$$

## 2.5. Size distribution and stability

### 2.5.1. Transmission electron microscopy

The transmission electron microscopy (TEM) images of the CUASL solution were observed using FEI Technai G2 120 kV instrument. The samples were diluted 100 times and were drop-cast in a carbon-coated copper grid (mesh size 200) from Icon Analyticals Pvt. Ltd, India and air-dried overnight.

### 2.5.2. Zeta potential and dynamic light scattering

The zeta potential and particle size measurements were done on the Brookhaven Instrument model 90 Plus Particle Size Analyzer and potential analyser. The zeta potential and average particle size of the CUASL nanostructures were determined with 100 times dilution.

## 2.6. Confocal microscopy

Laser scanning confocal microscopy from Zeiss was used for observing the stained cells. The microorganisms taken for this study were *S. aureus* ATCC 29737 (Gram-positive), *E. coli* NCIM 5129.

The overnight culture of the above microorganisms was set to OD 0.1. The cells were exposed to the fluorescent CUASL (5 w/v%) for not more than 2 h. The cells were washed to remove the unbound nanostructures and mounted on the coverslip, and glycerol was used as the mounting medium. The coverslip was sealed to prevent drying by evaporation. The slides were prepared freshly and visualized within 5 h. The excitation wavelength was 488 nm and emission was recorded at the wavelength range of 500–600 nm.

The images were processed using the Zen 2010 and ImageJ software. The fluorescence intensity of CUASL-treated cells, CTCF (corrected total cell fluorescence) was calculated using the following formula:

$$\text{CTCF} = \text{integrated density} - (\text{area of selected cell} \times \text{mean fluorescence of background readings}). \quad (2.6)$$

## 2.7. Quorum quenching assay

### 2.7.1. Bioluminescent reporter assay

Bioluminescence expression was quantified using a Tecan luminometer (Infinite M200, Männerdorf, Switzerland). An overnight culture of *E. coli* biosensor cells, pSB1142 (A kind gift from Prof. Williams, University of Nottingham, UK) was set to an OD600 nm of 0.2. Then, 200 µl of *E. coli* biosensor cells and CUASL (5 w/v%) having different concentrations of curcumin from 10 to 50 µg ml$^{-1}$ and ASL (5 w/v%) control were added into the well of 96-well microtiter plate. Expression of bioluminescence was measured in terms of relative light unit (RLU)/OD495 nm. Bioluminescence reduction in *E. coli* [pSB1142] explains the anti-QS properties of the CUASL nanostructures. CUASL (5 w/v%) and ASL (5 w/v%) at their respective concentrations were taken as control.

The quorum quenching activity of CUASL against *Pseudomonas aeruginosa* was done with the following assays. *Pseudomonas aeruginosa* NCIM 5029, used for the QQ assays, were grown in Luria Bertani media (LB) and maintained in glycerol stock at −20°C. ASL (5 w/v%) was taken as control for all the assays.

### 2.7.2. Anti-biofilm assay

CV biofilm assay was done in 96-well microtiter plate (MTP), as mentioned previously [58]. CUASL (5 w/v%) having different concentrations of curcumin from 10 to 50 µg ml$^{-1}$ were tested against biofilm formation at the 8th hr. The time point of the 8th hr was chosen because it is shown that the biofilm formation initiates at the 8th hr [59]. 200 µl of an overnight culture of *P. aeruginosa* was added to each well, set to OD 0.1 at 600 nm. The planktonic cells were removed and washed with distilled water twice and 200 µl of 0.1% crystal violet solution was added, and incubated for 15 min at room temperature. The excess crystal violet solution was discarded and 200 µl of 30% acetic acid solution was added to each of the wells. The reading was recorded at the absorbance of 580 nm.

### 2.7.3. Auto-aggregation assay

To understand the anti-adherence activity of CUASL, an overnight culture of *P. aeruginosa* was set to 0.1 OD at 660 nm. For this assay, the readings were recorded at the 8th hr. The OD at 660 nm at the 0th min was recorded and incubated at room temperature for 60 min. The OD at the 60th min was recorded at 660 nm. The auto-aggregation index was calculated as:

$$\text{auto-aggregation index} = \left(\frac{\text{OD}_{0\ \text{min}} - \text{OD}_{60\ \text{min}}}{\text{OD}_{0\ \text{min}}}\right). \quad (2.7)$$

### 2.7.4. Pyoverdine

The fluorescent siderophore, pyoverdine, is a quorum sensing mediated phenotype produced by *P. aeruginosa*. The inhibition of pyoverdine production was calculated by measuring the fluorescence. In 96-well MTP, 200 µL of *P. aeruginosa* (OD set to 0.1 at 600 nm) treated with CUASL at different concentrations (10–50 µg ml$^{-1}$) was added. The excitation wavelength of CUASL falls in the range of 470–570 nm (figure 2*b*), CUASL did not contribute to the measured pyoverdine fluorescence. The cells were excited at 405 nm and emission was recorded at 465 nm [60].

### 2.7.5. Pyocyanin

Pyocyanin is another exoproduct of *P. aeruginosa* synthesized by quorum sensing signalling. The overnight culture was set to 0.2 OD at 600 nm and CUASL was added at different concentrations

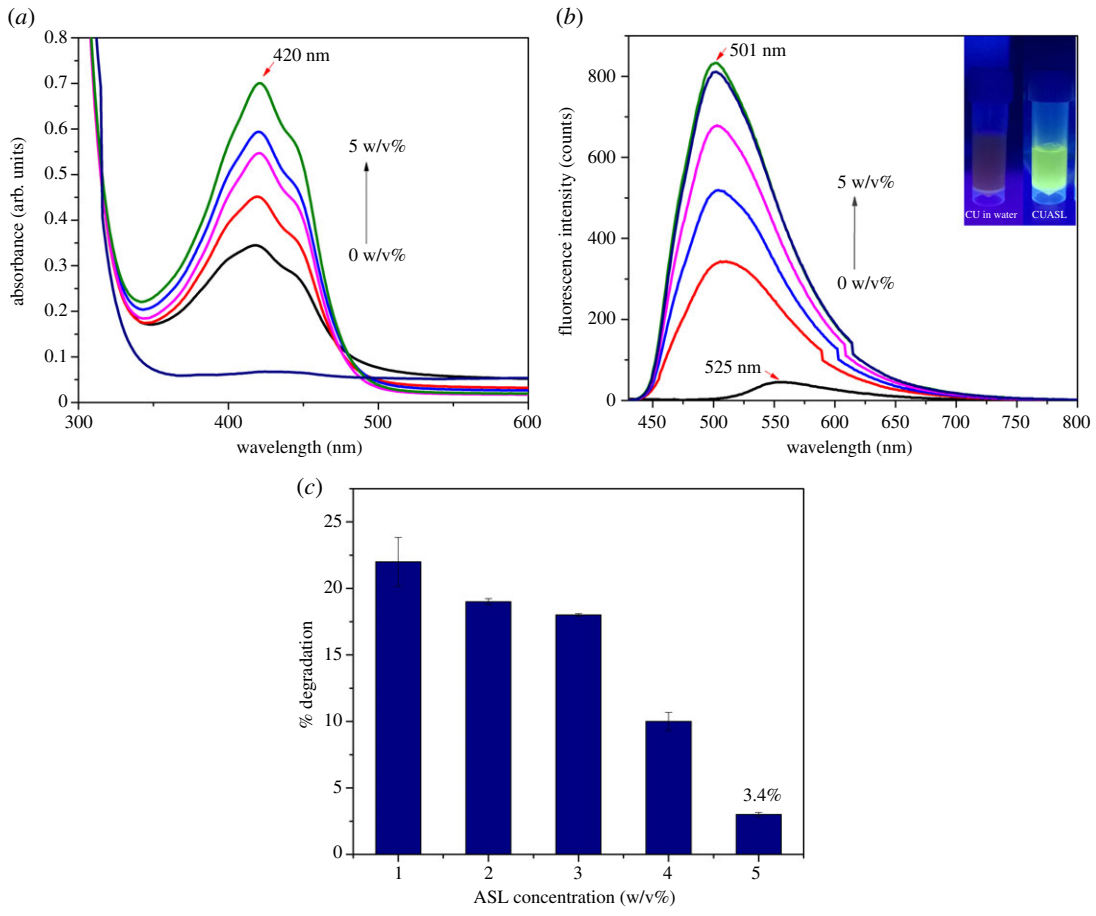


**Figure 2.** (*a*) Absorbance spectrum of CUASL at different ASL concentrations. As the concentration of ASL increases there is an increase in the intensity and peak shift to approximately 420 nm. (*b*) Emission spectrum of CUASL at different concentrations of ASL. A 24 nm peak shift can be observed with the increasing concentrations of ASL. Inset: green fluorescence of CUASL shown under UV transilluminator. (*c*) Degradation studies of curcumin at different ASL concentrations. At 5 w/v% of ASL, curcumin's degradation rate was reduced.

(10–50 µg ml$^{-1}$). The extraction of pyocyanin was done at the 24th hr by the following procedure. To the 5 ml of the cell-free supernatant, 3 ml chloroform and 1 ml 0.2 M HCl were added and centrifuged for 20 min at 8000 r.p.m. (28°C). The HCl layer was carefully separated and measured at OD 520 nm, keeping 0.2 M HCl as blank [61].

# 3. Results

## 3.1. Spectroscopic analysis

The spectrophotometric effect of ASL on curcumin was studied systematically at different concentrations from 1 to 5 w/v% (figure 2*a*). Structurally curcumin is a diferuloyl methane (figure 1) and exists as keto-enol isomer. In solutions, the enol form dominates the keto form [34]. A striking change in the absorption spectrum was observed in CUASL after the addition of ASL with increasing concentrations. The conjugated diferuloyl structure corresponds to the enol form, which is visualized at approximately 420 nm peak. The maximum absorption peak at approximately 420 nm indicates that it is due to the low-energy $\pi$-$\pi^*$ transition and curcumin is in its enolic form [62]. Curcumin is insoluble in water and hence absorption peak cannot be seen clearly, a similar trend for the curcumin in water was seen in our previous study [14]. A small shoulder at 440 nm can be observed in the presence of acidic sophorolipid. The peak shift and the 440 nm shoulder peak, as can be seen also in similar micellar systems, can be attributed to the shifting of curcumin from bulk to the micellar environment [24–27]. As previous literature suggests [24], this points us towards the location of curcumin in the palisade layer of the ASL micelles.

Steady-state fluorescence studies showed that the intensity of the curcumin fluorescence increases with the increase in the concentration of ASL (figure 2*b*). There was a blue shift ($\Delta\lambda_{fl} = 24$ nm) in

**Table 1.** Lifetime measurement parameters of CUASL (5 w/v% ASL concentration).

| CUASL (w/v%) | $\tau_1$ (ps) | $a_1$ | $\tau_2$ (ps) | $a_2$ | $\tau_3$ (ps) | $a_3$ | $\tau_{av}$ (ps) | $\chi^2$ |
|---|---|---|---|---|---|---|---|---|
| 0 | 18.5 | 0.66 | 106.7 | 0.33 | 523 | 0.01 | 52.651 | 0.98 |
| 5 | 89 | 0.54 | 406 | 0.32 | 1003 | 0.14 | 318.4 | 1.08 |

the fluorescence maximum ($\lambda_{fl}$) of CUASL ($\lambda_{fl} = 501$ nm) when compared with curcumin in water ($\lambda_{fl} = 525$ nm). This 24 nm blue shift in the emission spectrum indicated that curcumin is moving from the bulk phase into the micellar environment of ASL micelles. This blue shift can also be interpreted as hydrophobic interactions between curcumin and ASL micelles, similar to other micellar environments, especially TX-100 ($\lambda_{fl} = 501$ nm) [24].

When encapsulated with ASL micelles (pH ~4.5), curcumin was completely soluble, as opposed to the usual solubility of curcumin which is only possible at alkaline pH. A similar result was obtained when curcumin was solubilized in rhamnolipid micelles [63]. Rhamnolipids are glycolipid biosurfactants and are structurally similar to sophorolipids. This recent study showed that the interaction between the rhamnolipid and curcumin is pH dependent, and at acidic pH curcumin's stability was maintained. It has been understood that curcumin is stable at a pH range 1–6, because of the undissociated form of the hydroxyl groups [64]. About 80% of curcumin degrades in the aqueous buffer (pH 7.4) in a period of 60 min into vanillin, ferulic acid and feruloyl methane [65]. This degradation is attributed to the decrease in the absorption value. Thus, the degradation studies were conducted by recording the OD at the 0th and 60th min for different concentrations of ASL, to show that the acidic sophorolipid micelles minimize degradation of curcumin (figure 2*c*). At the concentration of 5 w/v%, the degradation of curcumin was as low as 3.4% and at the minimum concentration of 1 w/v%, 22.2%. Thus the spectroscopic and degradation studies showed that at 5 w/v%, curcumin was stable and the interaction with bulk water was minimized because of its encapsulation inside the ASL micelles. In addition to encapsulation, the pH of the ASL micellar system also contributes to the stability and reduced degradation of curcumin.

The above results revealed that the stability of the curcumin inside ASL micelles was concentration dependent and that 5 w/v% ASL was more stable with enhanced fluorescence. Thus, ASL micelles act as a drug carrier providing a stable environment for curcumin.

## 3.2. Lifetime and quantum yield measurements

Quantum yield and lifetime measurements are essential characteristics of a fluorophore. While quantum yield gives the information on the number of emitted photons relative to the absorbed photons, lifetime measurements provide the interaction time of the fluorophore with its environment. TCSPC is an excellent tool to understand the excited state dynamics. It is also useful to know the strength, stability and the layer in which the drug is bound to the micelle. The time-resolved study gives an idea of the drug location in the micelle and also details regarding the surrounding environment of the drug.

The quantum yield of curcumin-sophorolipid nanostructures at 5 w/v% was calculated by taking quinine sulphate in 0.1 M $H_2SO_4$ as the standard [38] and was found to be 0.014. Because of the effect of non-radiative decay, there was no marked difference in the quantum yield at different ASL concentrations. This observation was complemented by the lifetime measurements, as not much lifetime difference was witnessed at different ASL concentrations.

The decay profile (figure 3) of curcumin entrapped in 5 w/v% ASL micelles and water was recorded at 501 nm using the 400 nm diode laser source. As it is evident from the decay profile that curcumin in water is overlapped with the prompt, hence the decay is negligible. The decay for 5 w/v% was multi-exponential and was fit using triple exponentials. The average lifetime of CUASL was 318.5 ps with the fastest decay component at 89 ps, the slower component at 406 ps and longer-lived component at 1003 ps. The multiexponential nature of the decay indicates a complex nature of the interaction between curcumin and ASL micelles. This corroborates well with the absorption studies and confirmed that curcumin was entrapped in the palisade layer of the acidic sophorolipid micelles which is a mixed combination of sophorose, COOH, and aliphatic region along with water.

It is well known that the major photophysical event of curcumin is excited state intramolecular proton transfer (ESIPT). In the presence of non-polar solvents, the ESIPT process increases leading to a very short

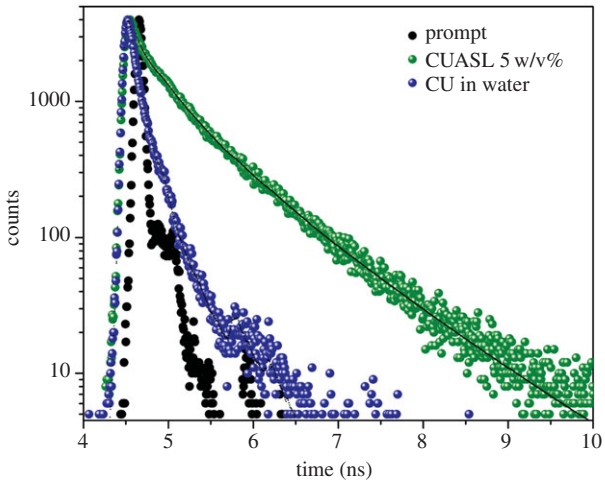


**Figure 3.** Lifetime measurement of CUASL (5 w/v%) and CU in water. There is an increase in lifetime with triple exponential decay in the presence of 5 w/v% ASL.

**Table 2.** Photophysical parameters of CUASL (5 w/v% ASL concentration).

| CUASL (w/v%) | $\lambda_a$ (nm) | $\lambda_{fl}$ (nm) | $\varphi_f$ | $\tau_{av}$ (ps) | $k_r/10^7$ ($s^{-1}$) | $k_{nr}/10^9$ ($s^{-1}$) |
|---|---|---|---|---|---|---|
| 0 | 430 | 525 | — | 52.651 | — | — |
| 5 | 420 | 501 | 0.014 | 318.5 | 4.39 | 3.09 |

lifetime (few hundred femtoseconds). On the other hand, in the polar solvents like acetone, the ESIPT process decreases and thereby increases the lifetime. A similar trend was seen in the case of CUASL nanostructures, the ESIPT was minimized, as it can be reflected by the longer lifetimes (figure 3). The increase in the lifetime was due to the ESIPT process hindrance that may be due to the intermolecular hydrogen bonding or hydrophobic interaction between the oleic acid moiety of the ASL and curcumin as pointed out previously [13].

The radiative and non-radiative decay kinetics were calculated, and the photophysical parameters were tabulated (table 2). The relatively low non-radiative decay constant ($k_{nr}$) and increase in the radiative decay constant ($k_r$) reinforces the hindrance in the ESIPT process after the addition of ASL. The results obtained are comparable with the polymeric micelles [27,28]. The higher lifetime value and amplified fluorescence intensity of CUASL, as compared to CU in water, can be ascribed to the increased radiative decay value ($k_r$).

## 3.3. Size distribution

The formed nanostructures were intact as seen from the TEM images (figure 4). The formed CUASL micelles were not perfectly spherical, rather a little elongated, forming ellipsoidal structures were approximately 100 nm size.

The above size was confirmed with dynamic light scattering (electronic supplementary material, figure S1) and the size distribution of around 100 nm with the polydispersity index of 0.27. This size was calculated in the solution whereas TEM characterization was done with air-dried sample. The polydispersity index and non-uniformity of TEM images confirmed that the micelles were dynamic, giving minor changes in the overall size of the nanostructures.

The stability of CUASL nanostructures was measured using zeta potential (electronic supplementary material, figure S1). The average zeta potential was −38.41 mV which indicated that the CUASL structures were quite stable. The above size distribution and stability analysis confirmed that formed CUASL nanostructures and their stability are complementary to the photophysical analysis.

The schematic representation of the CUASL nanostructures is shown in figure 5.

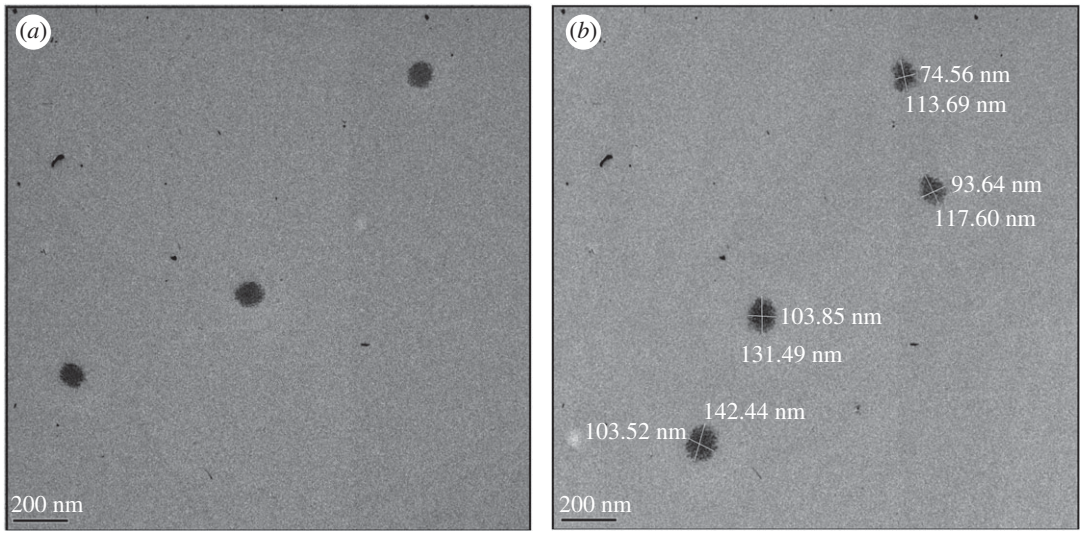


**Figure 4.** (*a*,*b*) TEM images of the formed CUASL nanostructures.

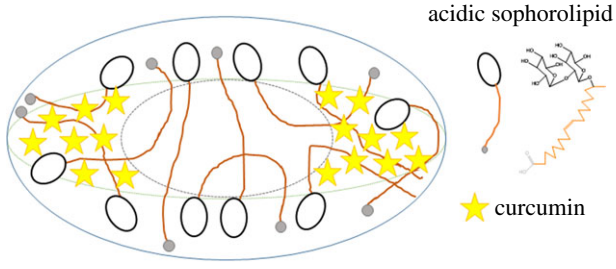


**Figure 5.** Schematic diagram representing the probable position of curcumin within the palisade layer of ASL micelles. ASL micelle structure was redrawn as given in the reference [12].

## 3.4. Confocal microscopy

The photophysical studies revealed that CUASL nanostructures have enhanced green fluorescence, which can be exploited for bioimaging applications. The confocal microscopic analysis was carried out to investigate the uptake of CUASL nanostructures by the bacterial cells. The confocal microscopic images (figures 6 and 7) showed bright green fluorescent bacterial cells. In the short time span of 2 h, the bacterial cells (both Gram-negative and Gram-positive) effectively internalized CUASL nanostructures.

CTCF was calculated for treated and untreated cells, and since untreated cells do not show fluorescence, the CTCF was near zero. And for the CUASL-treated cells, CTCF was calculated to be 48 241 intensity units for *E. coli* and 32 541 intensity units for *S. aureus*. The previous study on the synergistic action of sophorolipids and antibiotics speculated that the sophorolipids facilitate the entry of the antibiotics into the bacterial cell interior [66]. A similar mechanism can be extrapolated to CUASL nanostructures. Acidic sophorolipids have self-assembling properties and mimic the bacterial cell membrane. This helps to span through the cell membrane and thereby release curcumin inside the cytoplasm of the cell. It is interesting to note that the CUASL-treated cells, did not show any change in morphology, which visually indicates that the fluorescent CUASL nanostructures did not rupture the cells, and hence can be effectively used for bioimaging.

Curcumin was shown to be used as a fluorescent biomarker in mammalian uptake studies by using different solvents [40–44]. Though the quantum yield was low, bacterial cell uptake studies showed that CUASL can be tagged with specific markers; it can be used for selective imaging of different types of cells, exploring its use as a bioimaging tool.

Since the bacterial cells remained intact after the treatment of CUASL, it leads us to explore its biological activity.

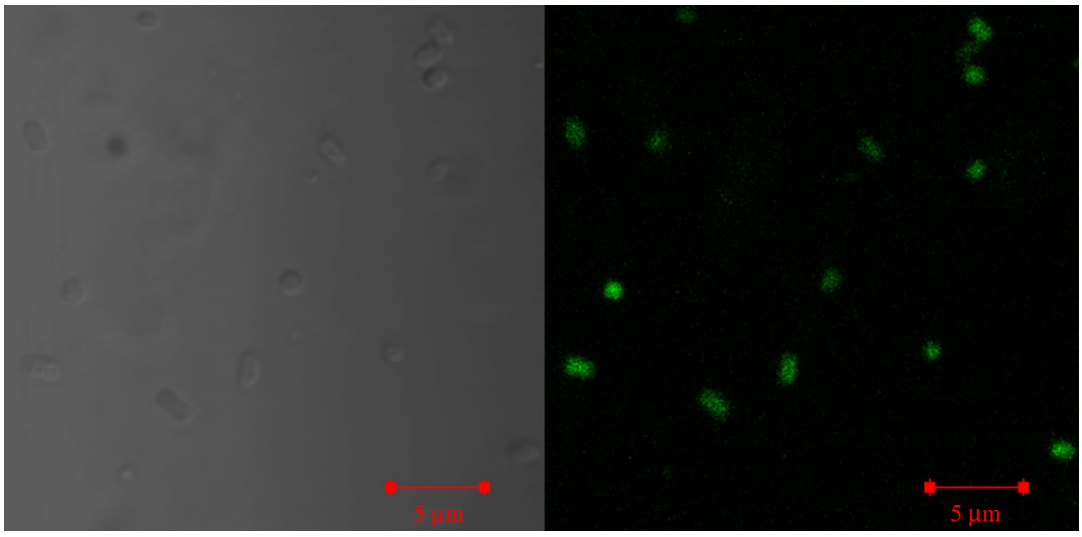


**Figure 6.** Confocal micrographs of *E. coli* treated with CUASL (5 w/v%). Left is the phase contrast image and right is the fluorescent image of the bacterial cells. The CUASL treatment has not ruptured the cells.

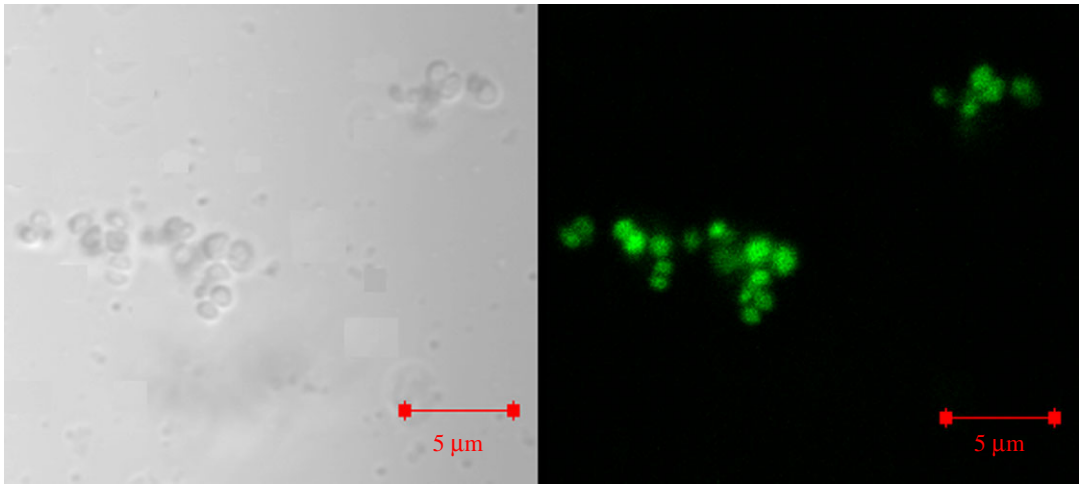


**Figure 7.** Confocal micrographs of *S. aureus* treated with CUASL (5 w/v%). Left is the phase contrast image and right is the fluorescent image of the bacterial cells. The CUASL treatment has not ruptured the cells.

## 3.5. Quorum quenching assays

### 3.5.1. Bioluminescent assay

The CUASL (5 w/v%) showed a significant reduction in bioluminescence, with the maximum inhibition at the concentration of 50 µg ml$^{-1}$. The signalling molecule used was 3-oxo-C12 HSL, which is specific to *P. aeruginosa*. The CUASL showed effective inhibition of 3-oxo-C12 HSL (electronic supplementary material, figure S2). This indicated that CUASL was bound to the signal receptor. It should be noted that ASL (5 w/v%) did not have any quorum quenching effect (data not shown). This helped us to proceed for checking quorum quenching activity of CUASL against *P. aeruginosa*.

### 3.5.2. Anti-biofilm and anti-adherence activity

The ability to form biofilm by bacteria is considered to be the most efficient escape mechanism from antibiotics. Biofilm formation is mediated through quorum sensing pathways. The biofilm formation for *P. aeruginosa* initiates at the 8th hr. Thus, for anti-biofilm activity, CUASL should act before the commencement of biofilm formation. The maximum biofilm inhibition of CUASL was recorded at

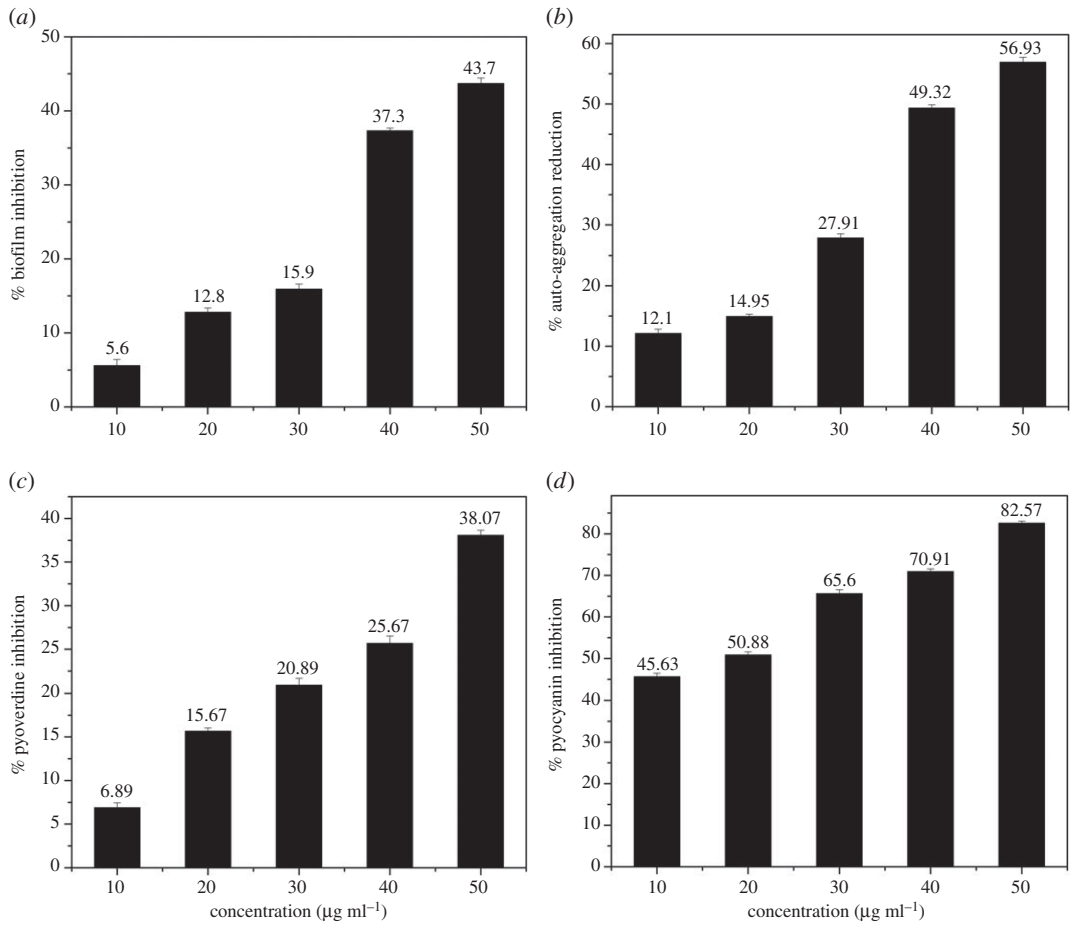


**Figure 8.** Quorum Quenching Activity of CUASL (5 w/v%) against *P. aeruginosa*: (*a*) anti-biofilm activity, (*b*) auto-aggregation reduction activity, (*c*) pyoverdine reduction, (*d*) pyocyanin reduction.

50 μg ml$^{-1}$ at the 8th hr. Previous reports have already proved that curcumin has anti-biofilm effects when dissolved in different solvents; ASL (5 w/v%) was taken as control and it did not have a significant anti-biofilm effect (data not shown) (figure 8*a*).

To understand the effect of adherence, auto-aggregation index was calculated at the same time point and concentration, as that of a biofilm. The auto-aggregation index matched exactly with the anti-biofilm activity. At the 8th hr and at 50 μg ml$^{-1}$ concentration of curcumin, 58% inhibition was observed in auto-aggregation. Thereby, the bacterial cells aggregation was inhibited (figure 8*b*). Bacterial aggregation leads to the biofilm formation. Thus CUASL acts as an anti-biofilm agent by perturbing the aggregation process.

### 3.5.3. Pyocyanin and pyoverdine assay

The exoproducts released by *P. aeruginosa* play a significant role in rendering resistance to antibiotics. The siderophore pyoverdine is an iron transporter which is linked to the biofilm formation and mediated through quorum sensing. As CUASL showed anti-biofilm activity, it is quite likely to perturb the pyoverdine synthesis as well. Hence the effect of CUASL on pyoverdine inhibition was tested. The CUASL facilitated pyoverdine inhibition at 50 μg ml$^{-1}$ concentration in 24 h. The decrease in the auto-fluorescence mediated by pyoverdine was observed (figure 8*c*).

Pyocyanin is a phenazine found in the sputum of *P. aeruginosa* infected patients. Its production is regulated under quorum sensing signalling. It generates reactive oxygen species and thus creates oxidative stress in healthy cells causing damage. When CUASL was tested against pyocyanin production, at 50 μg ml$^{-1}$ concentration of CUASL, pyocyanin was inhibited by almost 82% (figure 8*d*).

The virulent factors regulated by quorum sensing pathways of *P. aeruginosa* were attenuated by CUASL nanostructures, without inhibiting the growth. This suggests that CUASL nanostructures showed quorum quenching activity against *P. aeruginosa*.

# 4. Conclusion

The present study reports the use of acidic sophorolipid for solubilizing the hydrophobic drug, curcumin, by entrapping them inside micelles. The CUASL system was analysed using photophysical techniques like UV-Vis spectroscopy, fluorescence spectroscopy and lifetime measurements. In addition to making curcumin aqueous and soluble at an acidic pH, we have shown that ASL reduces the degradation of curcumin by hydrolysis by almost 95%. The enhanced green fluorescence of CUASL with the blue shift signifies the movement of curcumin into the ASL micellar environment. Lifetime and quantum yield measurements reveal that the encapsulation by ASL micelles changes the excited state dynamics and leads to the reduction in ESIPT (excited state intramolecular proton transfer). Since it was already shown in the previous literature that curcumin, as well as sophorolipid, have anti-biofilm activity, we have demonstrated that they work synergistically as a quorum quencher against *Pseudomonas aeruginosa* and finally, the property of fluorescence was extended as a biomarker agent for confocal imaging. The bright green fluorescence imparted to the bacterial cells opens up an area for the development of soluble curcumin-based bioimaging system. This is the first report of photophysical analysis of curcumin encapsulated inside biosurfactant micelles.

Data accessibility. The datasets, electronic supplementary material, figure S1: Zeta potential and DLS log summary of CUASL and electronic supplementary material, figure S2: Quorum quenching-Bioluminescence assay of CUASL supporting this article have been uploaded as part of the electronic supplementary material.

Authors' contributions. A.A.P.: conception, analysis of the data, revising and final approval of the version. S.V.: design of experiments, data analysis and interpretation, and drafting the article.

Competing interests. We declare that we have no competing interests.

Funding. We received no funding for this study.

Acknowledgements. Authors would like to thank Priti Darne (NCL, Pune) for the help of acidic sophorolipid purification and Amrita Patil (NCL, Pune) for QQ assays. We also thank Dr Partha Hazra (IISER, Pune) and Dr Amitava Das (NCL, Pune) for fluorescent measurements, Dr Richa Rikky and Vijay Vitthal (IISER, Pune) for Confocal Microscopy Measurements and Parul Dubey (NCL, Pune) for the help in the manuscript correction.

# References

1. Singh P, Cameotra SS. 2004 Potential applications of microbial surfactants in biomedical sciences. *Trends Biotechnol.* **22**, 142–146. (doi:10.1016/j.tibtech.2004.01.010)
2. Pontes C, Alves M, Santos C, Ribeiro MH, Gonçalves L, Bettencourt AF, Ribeiro IAC. 2016 Can sophorolipids prevent biofilm formation on silicone catheter tubes? *Int. J. Pharm.* **513**, 697–708. (doi:10.1016/j.ijpharm.2016.09.074)
3. Van Bogaert INA, Zhang J, Soetaert W. 2011 Microbial synthesis of sophorolipids. *Process Biochem.* **46**, 821–833. (doi:10.1016/j.procbio.2011.01.010)
4. Faivre V, Rosilio V. 2010 Interest of glycolipids in drug delivery: from physicochemical properties to drug targeting. *Expert Opin. Drug Deliv.* **7**, 1031–1048. (doi:10.1517/17425247.2010.511172)
5. Van Bogaert INA, Saerens K, De Muynck C, Develter D, Soetaert W, Vandamme EJ. 2007 Microbial production and application of sophorolipids. *Appl. Microbiol. Biotechnol.* **76**, 23–34. (doi:10.1007/s00253-007-0988-7)
6. García-Ochoa F, Casas JA. 1999 Unstructured kinetic model for sophorolipid production by *Candida bombicola*. *Enzyme Microb. Technol.* **25**, 613–621. (doi:10.1016/S0141-0229(99)00089-7)
7. Singh S, Patel P, Jaiswal S, Prabhune AA, Ramana C V., Prasad BLV. 2009 A direct method for the preparation of glycolipid–metal nanoparticle conjugates: sophorolipids as reducing and capping agents for the synthesis of water re-dispersible silver nanoparticles and their antibacterial activity. *New J. Chem.* **33**, 646–652. (doi:10.1039/B811829A)
8. Dubey P, Nawale L, Sarkar D, Nisal A, Prabhune A. 2015 Sophorolipid assisted tunable and rapid gelation of silk fibroin to form porous biomedical scaffolds. *RSC Adv.* **5**, 33 955–33 962. (doi:10.1039/C5RA04317D)
9. Dubey P, Kumar S, Aswal VK, Ravindranathan S, Rajamohanan PR, Prabhune A, Nisal A. 2016 Silk fibroin-sophorolipid gelation: deciphering the underlying mechanism. *Biomacromolecules* **17**, 3318–3327. (doi:10.1021/acs.biomac.6b01069)
10. Fariya M, Jain A, Dhawan V, Shah S, Nagarsenker MS. 2014 Bolaamphiphiles: a pharmaceutical review. *Adv. Pharm. Bull.* **4**, 483–491. (doi:10.5681/apb.2014.072)
11. Baccile N, Babonneau F, Jestin J, Pehau-Arnaudet G, Van Bogaert I. 2012 Unusual, pH-induced, self-assembly of sophorolipid biosurfactants. *ACS Nano* **6**, 4763–4776. (doi:10.1021/nn204911k)
12. Manet S, Cuvier A-S, Valotteau C, Fadda GC, Perez J, Karakas E, Abel S, Baccile N. 2015 Structure of bolaamphiphile sophorolipid micelles characterized with SAXS, SANS, and MD simulations. *J. Phys. Chem. B* **119**, 13 113–13 133. (doi:10.1021/acs.jpcb.5b05374)
13. Singh PK, Wani K, Kaul-Ghanekar R, Prabhune A, Ogale S. 2014 From micron to nano-curcumin by sophorolipid co-processing: highly enhanced bioavailability, fluorescence, and anti-cancer efficacy. *RSC Adv.* **4**, 60 334–60 341. (doi:10.1039/C4RA07300B)
14. Darne PA, Mehta MR, Agawane SB, Prabhune AA. 2016 Bioavailability studies of curcumin–sophorolipid nano-conjugates in the aqueous phase: role in the synthesis of uniform gold nanoparticles. *RSC Adv.* **6**, 68 504–68 514. (doi:10.1039/C6RA13469F)
15. Motterlini R, Foresti R, Bassi R, Green CJ. 2000 Curcumin, an antioxidant and anti-inflammatory agent, induces heme oxygenase-1 and protects endothelial cells against oxidative stress. *Free Radic. Biol. Med.* **28**, 1303–1312. (doi:10.1016/S0891-5849(00)00294-X)
16. Zorofchian Moghadamtousi S, Abdul Kadir H, Hassandarvish P, Tajik H, Abubakar S, Zandi K. 2014 A review on antibacterial, antiviral, and antifungal activity of curcumin. *Biomed Res. Int.* **2014**, 1–12. (doi:10.1155/2014/186864)
17. Thiyagarajan M, Sharma SS. 2004 Neuroprotective effect of curcumin in middle cerebral artery occlusion induced focal cerebral ischemia in rats. *Life Sci.* **74**, 969–985. (doi:10.1016/j.lfs.2003.06.042)
18. Reddy RC, Vatsala PG, Keshamouni VG, Padmanaban G, Rangarajan PN. 2005 Curcumin for malaria therapy. *Biochem. Biophys. Res. Commun.* **326**, 472–474. (doi:10.1016/j.bbrc.2004.11.051)
19. Kuttan G, Hari Kumar KB, Guruvayoorappan C, Kuttan R. 2007 Antitumor, anti-invasion, and antimetastatic effects of curcumin. In *The molecular targets and therapeutic uses of curcumin in health and disease* (eds BB Aggarwal, Y-J Surh, S Shishodia), pp. 173–184. Advances in experimental medicine and biology, vol. 595. Boston, MA: Springer US.
20. López-Lázaro M. 2008 Anticancer and carcinogenic properties of curcumin: considerations for its

clinical development as a cancer chemopreventive and chemotherapeutic agent. *Mol. Nutr. Food Res.* **52**, 103–127. (doi:10.1002/mnfr.200700238)

21. Gururaj AE, Belakavadi M, Venkatesh DA, Marmé D, Salimath BP. 2002 Molecular mechanisms of anti-angiogenic effect of curcumin. *Biochem. Biophys. Res. Commun.* **297**, 934–942. (doi:10.1016/S0006-291X(02)02306-9)
22. Bhandarkar SS, Arbiser JL. 2007 Curcumin as an inhibitor of angiogenesis. In *The molecular targets and therapeutic uses of curcumin in health and disease* (eds BB Aggarwal, Y-J Surh, S Shishodia), pp. 185–195. Advances in experimental medicine and biology, vol. 595. Boston, MA: Springer US.
23. Rachmawati H. 2013 Curcumin nanoforms promise better therapeutic values. *Int. J. Res. Pharm. Sci.* **4**, 211–220.
24. Adhikary R, Carlson PJ, Kee TW, Petrich JW. 2010 Excited-state intramolecular hydrogen atom transfer of curcumin in surfactant micelles. *J. Phys. Chem. B* **114**, 2997–3004. (doi:10.1021/jp9101527)
25. Sharma R, Jani D. 2013 Interaction of cationic CTAB surfactant with curcumin, an anticarcinogenic drug: spectroscopic investigation. *Tenside Surfactants Deterg.* **50**, 283–288. (doi:10.3139/113.110261)
26. Boruah B, Saikia PM, Dutta RK. 2012 Binding and stabilization of curcumin by mixed chitosan-surfactant systems: a spectroscopic study. *J. Photochem. Photobiol. A Chem.* **245**, 18–27. (doi:10.1016/j.jphotochem.2012.07.004)
27. Banerjee C, Ghosh S, Mandal S, Kuchlyan J, Kundu N, Sarkar N. 2014 Exploring the photophysics of curcumin in zwitterionic micellar system: an approach to control ESIPT process in the presence of room temperature ionic liquids (RTILs) and anionic surfactant. *J. Phys. Chem. B* **118**, 3669–3681. (doi:10.1021/jp411778q)
28. Banerjee C, Maiti S, Mustafi M, Kuchlyan J, Banik D, Kundu N, Dhara D, Sarkar N. 2014 Effect of encapsulation of curcumin in polymeric nanoparticles: how efficient to control ESIPT process? *Langmuir* **30**, 10 834–10 844. (doi:10.1021/la5023533)
29. Baglole KN, Boland PG, Wagner BD. 2005 Fluorescence enhancement of curcumin upon inclusion into parent and modified cyclodextrins. *J. Photochem. Photobiol. A Chem.* **173**, 230–237. (doi:10.1016/j.jphotochem.2005.04.002)
30. Tønnesen HH, Másson M, Loftsson T. 2002 Studies of curcumin and curcuminoids. XXVII. Cyclodextrin complexation: solubility, chemical and photochemical stability. *Int. J. Pharm.* **244**, 127–135. (doi:10.1016/S0378-5173(02)00323-X)
31. Tang B, Ma L, Wang H, Zhang G. 2002 Study on the supramolecular interaction of curcumin and $\beta$-cyclodextrin by spectrophotometry and its analytical application. *J. Agric. Food Chem.* **50**, 1355–1361. (doi:10.1021/jf0111965)
32. Barik A, Priyadarsini KI, Mohan H. 2003 Photophysical studies on binding of curcumin to bovine serum albumins. *Photochem. Photobiol.* **77**, 597–603. (doi:10.1562/0031-8655(2003)077<0597:PSOBOC>2.0.CO;2)
33. Barik A, Mishra B, Kunwar A, Indira Priyadarsini K. 2007 Interaction of curcumin with human serum albumin: thermodynamic properties, fluorescence energy transfer and denaturation effects. *Chem. Phys. Lett.* **436**, 239–243. (doi:10.1016/j.cplett.2007.01.006)
34. El Khoury ED, Patra D. 2013 Ionic liquid expedites partition of curcumin into solid gel phase but discourages partition into liquid crystalline phase of 1,2-dimyristoyl-sn-glycero-3-phosphocholine liposomes. *J. Phys. Chem. B* **117**, 9699–9708. (doi:10.1021/jp4061413)
35. Patra D, Riwa A, Kamal B. 2013 Fluorometric sensing of DNA using curcumin encapsulated in nanoparticle-assembled microcapsules prepared from poly(diallylammonium chloride-co-sulfur dioxide). *Microchim. Acta* **180**, 59–64. (doi:10.1007/s00604-012-0903-5)
36. Mouslmani M, Patra D. 2014 Revoking excited state intra-molecular hydrogen transfer by size dependent tailor-made hierarchically ordered nanocapsules. *RSC Adv.* **4**, 8317–8320. (doi:10.1039/c3ra45095c)
37. Chebl M, Abiad MG, Moussa Z, Patra D. 2016 Two modes of associations of curcumin with pre- and nanoaggregated chitosan oligosaccharide lactate: ionic strength and hydrophobic bile salt modulate partition of drug and self-assembly process. *J. Phys. Chem. C* **20**, 11 210–11 224. (doi:10.1021/acs.jpcc.6b01486)
38. Khopde SM, Priyadarsini KI, Palit DK, Mukherjee T. 2000 Effect of solvent on the excited-state photophysical properties of curcumin. *Photochem. Photobiol.* **72**, 625–631. (doi:10.1562/0031-8655(2000)0720625eosote2.0.co2)
39. Kumar A, Li L, Chaturvedi A, Brzostowski J, Chittigori J, Pierce S, Samuelson LA, Sandman D, Kumar J. 2012 Two-photon fluorescence properties of curcumin as a biocompatible marker for confocal imaging. *Appl. Phys. Lett.* **100**, 10–14. (doi:10.1063/1.4717753)
40. Park K, Seo Y, Kim MK, Kim K, Kim YK, Choo H, Chong Y. 2015 A curcumin-based molecular probe for near-infrared fluorescence imaging of tau fibrils in Alzheimer's disease. *Org. Biomol. Chem.* **13**, 11 194–11 199. (doi:10.1039/C5OB01847A)
41. Kunwar A, Barik A, Mishra B, Priyadarsini KI, Rathinasamy K, Pandey R. 2007 Differential up-take and fluorescence of curcumin, a yellow pigment from turmeric, in normal vs tumor cells. *BARC Newsletter* **285**, 202–207.
42. Kunwar A, Barik A, Mishra B, Rathinasamy K, Pandey R, Priyadarsini KI. 2008 Quantitative cellular uptake, localization and cytotoxicity of curcumin in normal and tumor cells. *Biochim. Biophys. Acta - Gen. Subj.* **1780**, 673–679. (doi:10.1016/j.bbagen.2007.11.016)
43. Harada T *et al.* 2013 Diamide linked $\gamma$-cyclodextrin dimers as molecular-scale delivery systems for the medicinal pigment curcumin to prostate cancer cells. *Mol. Pharm.* **10**, 4481–4490. (doi:10.1021/mp400309s)
44. Zhang X *et al.* 2015 Curcumin analogues as selective fluorescence imaging probes for brown adipose tissue and monitoring browning. *Sci. Rep.* **5**, 13116. (doi:10.1038/srep13116)
45. Tyagi P, Singh M, Kumari H, Kumari A, Mukhopadhyay K. 2015 Bactericidal activity of curcumin I is associated with damaging of bacterial membrane. *PLoS ONE* **10**, 1–15. (doi:10.1371/journal.pone.0121313)
46. Uroz S, Dessaux Y, Oger P. 2009 Quorum sensing and quorum quenching: the yin and yang of bacterial communication. *ChemBioChem* **10**, 205–216. (doi:10.1002/cbic.200800521)
47. Juhas M, Eberl L, Tummler B. 2005 Quorum sensing: the power of cooperation in the world of *Pseudomonas*. *Environ. Microbiol.* **7**, 459–471. (doi:10.1111/j.1462-2920.2005.00769.x)
48. Schuster M, Peter Greenberg E. 2006 A network of networks: quorum-sensing gene regulation in *Pseudomonas aeruginosa*. *Int. J. Med. Microbiol.* **296**, 73–81. (doi:10.1016/j.ijmm.2006.01.036)
49. Rudrappa T, Bais HP. 2008 Curcumin, a known phenolic from *Curcuma longa*, attenuates the virulence of *Pseudomonas aeruginosa* PAO1 in whole plant and animal pathogenicity models. *J. Agric. Food Chem.* **56**, 1955–1962. (doi:10.1021/jf072591j)
50. Jadaun V, Prateeksha P, Singh BR, Paliya BS, Upreti DK, Rao CV, Rawat AKS, Singh BN. 2015 Honey enhances the anti-quorum sensing activity and anti-biofilm potential of curcumin. *RSC Adv.* **5**, 71 060–71 070. (doi:10.1039/C5RA14427B)
51. Lade H, Paul D, Kweon JH. 2015 Combined effects of curcumin and (−)-epigallocatechin gallate on inhibition of N-acylhomoserine lactone-mediated biofilm formation in wastewater bacteria from membrane bioreactor. *J. Microbiol. Biotechnol.* **25**, 1908–1919. (doi:10.4014/jmb.1506.06010)
52. Packiavathy IASV, Priya S, Pandian SK, Ravi AV. 2014 Inhibition of biofilm development of uropathogens by curcumin—an anti-quorum sensing agent from *Curcuma longa*. *Food Chem.* **148**, 453–460. (doi:10.1016/j.foodchem.2012.08.002)
53. Packiavathy IASV, Sasikumar P, Pandian SK, Veera Ravi A. 2013 Prevention of quorum-sensing-mediated biofilm development and virulence factors production in *Vibrio* spp. by curcumin. *Appl. Microbiol. Biotechnol.* **97**, 10 177–10 187. (doi:10.1007/s00253-013-4704-5)
54. Brackman G, Hillaert U, Van Calenbergh S, Nelis HJ, Coenye T. 2009 Use of quorum sensing inhibitors to interfere with biofilm formation and development in *Burkholderia multivorans* and *Burkholderia cenocepacia*. *Res. Microbiol.* **160**, 144–151. (doi:10.1016/j.resmic.2008.12.003)
55. Baccile N, Cuvier AS, Valotteau C, Van Bogaert INA. 2013 Practical methods to reduce impurities for gram-scale amounts of acidic sophorolipid biosurfactants. *Eur. J. Lipid Sci. Technol.* **115**, 1404–1412. (doi:10.1002/ejlt.201300131)
56. Imura T, Masuda Y, Minamikawa H, Fukuoka T, Konishi M, Morita T, Sakai H, Abe M, Kitamoto D. 2010 Enzymatic conversion of diacetylated sophoroselipid into acetylated glucoselipid: surface-active properties of novel bolaform biosurfactants. *J. Oleo Sci.* **59**, 495–501. (doi:10.5650/jos.59.495)
57. Satpathi S, Gavvala K, Hazra P. 2015 Fluorescence up-conversion studies of [2,2′-bipyridyl]-3,3′-diol in octyl-$\beta$-D-glucoside and other micellar aggregates. *J. Phys. Chem. A* **119**, 12 715–12 721. (doi:10.1021/acs.jpca.5b09832)
58. O'Toole GA. 2011 Microtiter dish biofilm formation assay. *J. Vis. Exp.* 3–5. (doi:10.3791/2437)
59. Rasamiravaka T, Labtani Q, Duez P, El Jaziri M. 2015 The formation of biofilms by *Pseudomonas aeruginosa*: a review of the natural and synthetic compounds interfering with control mechanisms. *Biomed Res. Int.* **2015**, 1–17. (doi:10.1155/2015/759348)

60. Mukherji R, Prabhune A. 2015 A new class of bacterial quorum sensing antagonists: glycomonoterpenols synthesized using linalool and alpha terpineol. *World J. Microbiol. Biotechnol.* **31**, 841–849. (doi:10.1007/s11274-015-1822-5)
61. Vijendra Kumar N, Murthy PS, Manjunatha JR, Bettadaiah BK. 2014 Synthesis and quorum sensing inhibitory activity of key phenolic compounds of ginger and their derivatives. *Food Chem.* **159**, 451–457. (doi:10.1016/j.foodchem.2014.03.039)
62. Shen L, Ji H-F. 2007 Theoretical study on physicochemical properties of curcumin. *Spectrochim. Acta Part A* **67**, 619–623. (doi:10.1016/j.saa.2006.08.018)
63. Moussa Z, Chebl M, Patra D. 2017 Fluorescence of tautomeric forms of curcumin in different pH and biosurfactant rhamnolipids systems: application towards on-off ratiometric fluorescence temperature sensing. *J. Photochem. Photobiol. B* **173**, 307–317. (doi:10.1016/j.jphotobiol.2017.06.011)
64. Esatbeyoglu T, Huebbe P, Ernst IMA, Chin D, Wagner AE, Rimbach G. 2012 Curcumin—from molecule to biological function. *Angew. Chemie Int. Ed.* **51**, 5308–5332. (doi:10.1002/anie.201107724)
65. Khurana A, Ho C-T. 1988 High performance liquid chromatographic analysis of curcuminoids and their photo-oxidative decomposition compounds in *Curcuma Longa L. J. Liq. Chromatogr.* **11**, 2295–2304. (doi:10.1080/01483918808067200)
66. Joshi-Navare K, Prabhune A. 2013 A biosurfactant-sophorolipid acts in synergy with antibiotics to enhance their efficiency. *Biomed Res. Int.* **2013**, 1–8. (doi:10.1155/2013/512495)